

Treatment of material discontinuity in two meshless local Petrov–Galerkin (MLPG) formulations of axisymmetric transient heat conduction

R. C. Batra^{*,†}, M. Porfiri and D. Spinello

Department of Engineering Science and Mechanics, MC 0219 Virginia Polytechnic Institute and State University, Blacksburg, VA 24061, U.S.A.

SUMMARY

We use two meshless local Petrov–Galerkin (MLPG) formulations to analyse heat conduction in a bimetallic circular disk. The continuity of the normal component of the heat flux at the interface between two materials is satisfied either by the method of Lagrange multipliers or by using a jump function. The convergence of the H^0 and H^1 error norms for the four numerical solutions with an increase in the number of equally spaced nodes and in the number of quadrature points is scrutinized. With an increase in the number of uniformly spaced nodes, the two error norms decrease monotonically for the MLPG5 formulation but are essentially unchanged for the MLPG1 formulation. To our knowledge, this is the first study comparing the performance of the two methods of modelling a discontinuity in the gradient of a field variable at the interface between two different materials. Copyright © 2004 John Wiley & Sons, Ltd.

KEY WORDS: meshless MLPG1 and MLPG5 methods; jump function; Lagrange multipliers; convergence studies

1. INTRODUCTION

Meshless methods such as the element-free Galerkin [1], hp-clouds [2], the reproducing kernel particle [3], the smoothed particle hydrodynamics [4], the diffuse element [5], the partition of unity finite element [6], the natural element [7], meshless Galerkin using radial basis functions [8], the meshless local Petrov–Galerkin (MLPG) [9], and the modified smoothed particle hydrodynamics (MSPH) [10] for seeking approximate solutions of partial differential equations have become popular during the last two decades because of the flexibility of placing nodes at arbitrary locations and the ability to treat the evolution of cracks. Many of these methods employ basis functions obtained by the moving least squares (MLS) technique of Lancaster

*Correspondence to: R. C. Batra, Department of Engineering Science and Mechanics, MC 0219 Virginia Polytechnic Institute and State University, Blacksburg, VA 24061, U.S.A.

†E-mail: rbatra@vt.edu

Received 22 August 2003

Revised 3 March 2004

Accepted 7 May 2004

and Salkauskas [11] to approximate the trial solution, and a background mesh to numerically evaluate integrals appearing in the weak formulation of a problem. However, in the MLPG method no background mesh is used to evaluate integrals appearing in the local weak formulation of the problem. The MLS basis functions are generally continuously differentiable over the entire domain which results in continuous derivatives of the trial solution. Thus for thermoelastic problems for a monolithic body, stresses, strains and the temperature are continuous throughout the body.

In the MLPG method, a weak formulation (or a weighted residual formulation) is derived over a subdomain, Ω_s , of the domain, Ω , of study. By repeated use of the divergence theorem, some or all of the spatial derivatives on the trial solution are transferred to the test function. For problems governed by second-order partial or ordinary differential equations, Atluri and Shen [12] have proposed six different choices of the test (or the weight) function and numbered the corresponding formulations as MLPG1, MLPG2, . . . , MLPG6. The MLPG1, MLPG5 and MLPG6 have first-order derivatives of the test function and the trial solution. The MLPG6 is the meshless local Galerkin formulation of an initial-boundary-value problem; it uses a MLS basis function as the test function, and results in symmetric mass and stiffness matrices. However, because of the considerable amount of CPU time required to find the MLS basis functions, it is computationally expensive. In MLPG5, the test function is a Heaviside unit step function on Ω_s and is generally less CPU intensive than the MLPG1 in which the test function equals a weight function appearing in the MLS basis functions for the trial solution but with Ω_s as its support.

For the Poisson equation, Atluri and Shen [12] have shown that the MLPG5 requires less computational effort than either the MLPG1 or the MLPG6 or the Galerkin finite element method (FEM). Qian *et al.* [13] compared the performance of the MLPG1 and the MLPG5 formulations for static deformations of a thick plate modelled by a compatible higher-order shear and normal deformable plate theory of Batra and Vidoli [14]. Both formulations gave results in close agreement with those either available in the literature or found from the analysis of the three-dimensional problem by FEM. With an increase in the number of equally spaced nodes in a square plate, and the number of quadrature points used to evaluate integrals numerically, displacements and stresses computed with the MLPG1 formulation converged monotonically to their 'exact' values and those with the MLPG5 method exhibited oscillations. Raju and Phillips [15] have compared the performances of the MLPG1 and the MLPG5 formulations for a beam problem governed by a fourth-order ordinary differential equation. Xiao and McCarthy [16] have used the multiquadratic radial basis functions and the MLPG5 formulation to analyse elastostatic problems.

Gu and Liu [17], Batra and Ching [18] and Qian *et al.* [19] have used the MLPG1 formulation and the Newmark family of methods to study, respectively, forced vibrations of a beam, plane strain elastodynamic deformations of a prenotched/precracked plate, and forced vibrations of homogeneous and functionally graded (FG) thick plates. Qian and Batra [20–22] have employed the MLPG1 formulation and the higher-order plate theory of Batra and Vidoli [14] to analyse transient thermoelastic deformations of a thick FG plate and to find the volume fractions of two constituents that optimize the first or the second natural frequency of a cantilever FG plate.

The continuity of derivatives of the MLS basis functions throughout the domain necessitates the use of special techniques to solve problems for an inhomogeneous body in which the continuity of surface tractions and/or the normal component of the heat flux requires that the derivative of displacements and/or temperature normal to an interface between two materials

be discontinuous. For the analysis of linear elastostatic problems by the element free Galerkin method, Cordes and Moran [23] used the method of Lagrange multipliers, and Krongauz and Belytschko [24] employed a special jump function at the line or the surface of discontinuity with parameters governing the strength of the discontinuity. Whereas Cordes and Moran studied a two-dimensional elastostatics problem, Krongauz and Belytschko analysed a one-dimensional elastostatics problem. Here we apply these two methods to the same problem and delineate their performances. Furthermore, two meshless, MLPG1 and MLPG5, formulations of an initial-boundary-value problem that corresponds to axisymmetric transient heat conduction in a circular bimetallic disk are used; thus the same one-dimensional problem is analysed by four methods. Warlock *et al.* [25] studied plane strain static deformations of a linear elastic body by the MLPG1 formulation and used the method of Lagrange multipliers to enforce contact conditions between a rough rigid wall and the elastic body.

The paper is organized as follows. Section 2 gives the governing equations, the MLS basis functions, the two MLPG formulations with the discontinuity in the temperature gradient at the interface modelled by a jump function and the continuity of the heat flux enforced by the method of Lagrange multipliers, and the generalized trapezoidal algorithm for integrating the coupled ordinary differential equations. The computation and discussion of results are given in Section 3. Results of this investigation are summarized in Section 4.

2. FORMULATION OF THE PROBLEM

2.1. Governing equations

We study transient heat conduction in a circular disk of radius R with the inner part of radius b made of one material and the annular disk of inner and outer radii b and R made of a different material; (cf. Figure 1). The two disks are perfectly bonded together at the circular surface $r = b$. A uniformly distributed heat source of intensity h is applied to the disk, and its outer edge is maintained at a uniform temperature T_0 . The initial temperature of the disk is at most a function of the radial co-ordinate r . Because of the symmetry of the geometry, and the initial and the boundary conditions, we assume that the temperature distribution is axisymmetric.

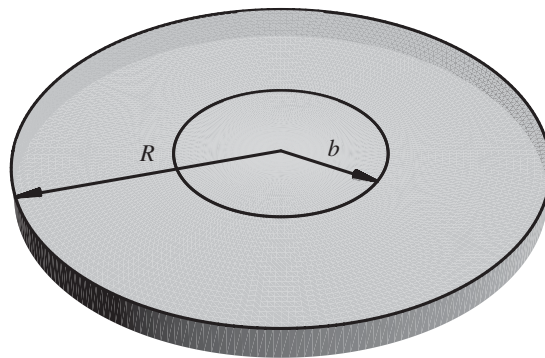


Figure 1. Schematic sketch of the problem studied.

It is governed by

$$\begin{aligned} \rho_1 c_1 \frac{\partial T_1}{\partial t} - \frac{1}{r} \frac{\partial}{\partial r} \left(r \kappa_1 \frac{\partial T_1}{\partial r} \right) &= h, \quad r \in (0, b), \quad t > 0 \\ \rho_2 c_2 \frac{\partial T_2}{\partial t} - \frac{1}{r} \frac{\partial}{\partial r} \left(r \kappa_2 \frac{\partial T_2}{\partial r} \right) &= h, \quad r \in (b, R), \quad t > 0 \end{aligned} \quad (1)$$

subject to the boundary conditions

$$\begin{aligned} \frac{\partial T_1}{\partial r}(0, t) &= 0, \quad t > 0 \\ \kappa_1 \frac{\partial T_1}{\partial r}(b^-, t) &= \kappa_2 \frac{\partial T_2}{\partial r}(b^+, t), \quad t > 0 \\ T_1(b, t) &= T_2(b, t), \quad t > 0 \\ T_2(R, t) &= T_0, \quad t > 0 \end{aligned} \quad (2)$$

and initial conditions

$$\begin{aligned} T_1(r, 0) &= T_1^0(r), \quad r \in [0, b] \\ T_2(r, 0) &= T_2^0(r), \quad r \in [b, R] \\ T_1^0(b) &= T_2^0(b), \quad \kappa_1 \left. \frac{dT_1^0}{dr} \right|_{r=b^-} = \kappa_2 \left. \frac{dT_2^0}{dr} \right|_{r=b^+} \end{aligned} \quad (3)$$

Here ρ is the mass density, c the specific heat, κ the thermal conductivity, t the time, T the temperature, and subscripts 1 and 2 denote quantities for materials 1 and 2, respectively. Equation (2)₁ follows from the symmetry of the problem. Equations (2)₂ and (2)₃ imply that the heat flux and the temperature at the common interface $r = b$ between the two materials are continuous. Since $\kappa_1 \neq \kappa_2$, therefore $\partial T / \partial r$ must be discontinuous at $r = b$. Boundary conditions (2)₁ and (2)₂ are natural, and (2)₃ and (2)₄ are essential.

2.2. Moving least squares (MLS) basis functions

Let N nodes be located at r_1, r_2, \dots, r_N in $[0, R]$ with $r_1 = 0$, and $r_N = R$, and $T^h(r, t)$ be the trial solution defined on a subdomain $\Omega_s \subset [0, R]$. Following Lancaster and Salkauskas [11], we write

$$T^h(r, t) = \sum_{j=1}^m p_j(r) a_j(r, t) \quad (4)$$

where

$$\mathbf{p}^T(r) = \{1, r, r^2, \dots, r^{m-1}\} \quad (5)$$

is a complete monomial in r of degree $m - 1$. The unknown coefficients $a_1(r, t), a_2(r, t), \dots, a_m(r, t)$ are determined by minimizing J defined by

$$J = \sum_{i=1}^N W(r - r_i) [\mathbf{p}^T(r_i) \mathbf{a}(r, t) - \hat{T}_i(t)] \tag{6}$$

where $\hat{T}_i(t)$ is the time-dependent fictitious value of T at the point $r = r_i$. Note that the number, n , of nodes for which the non-negative weight function $W(r - r_i) > 0$ at the point with the radial co-ordinate r is much less than N . Belytschko *et al.* [1] have discussed requirements to be imposed on the weight function W and several choices for it; here we take it to be a fourth-order spline function

$$W(r - r_i) = \begin{cases} 1 - 6 \left(\frac{d_i}{r_w}\right)^2 + 8 \left(\frac{d_i}{r_w}\right)^3 - 3 \left(\frac{d_i}{r_w}\right)^4, & 0 \leq d_i \leq r_w \\ 0, & d_i > r_w \end{cases} \tag{7}$$

where $d_i = |r - r_i|$, and $2r_w$ equals the support of the weight function W .

The stationarity of J with respect to $\mathbf{a}(r, t)$ yields

$$\mathbf{A}(r) \mathbf{a}(r, t) = \mathbf{B}(r) \hat{\mathbf{T}}(t) \tag{8}$$

where

$$\begin{aligned} \mathbf{A}(r) &= \sum_{i=1}^N W(r - r_i) \mathbf{p}^T(r_i) \mathbf{p}(r_i) \\ \mathbf{B}(r) &= [W(r - r_1) \mathbf{p}(r_1), W(r - r_2) \mathbf{p}(r_2), \dots, W(r - r_N) \mathbf{p}(r_N)] \end{aligned} \tag{9}$$

Matrices \mathbf{A} and \mathbf{B} are $m \times m$ and $m \times N$ respectively. However, because of several columns in \mathbf{B} of zeros, its size can be reduced to $m \times n$. Solving the linear system of Equation (8) for \mathbf{a} and substituting the result in (4) we obtain

$$T^h(r, t) = \sum_{j=1}^N \phi_j(r) \hat{T}_j(t) \tag{10}$$

where

$$\phi_k(r) = \sum_{j=1}^m p_j(r) [\mathbf{A}^{-1}(r) \mathbf{B}(r)]_{jk} \tag{11}$$

are the basis functions of the MLS approximation. Lancaster and Salkauskas [11] have shown that $1, r, r^2, \dots, r^{m-1}$ can be exactly represented as a linear combination of $\phi_1, \phi_2, \dots, \phi_m$. In order for the matrix \mathbf{A} defined by Equation (9)₁ to be invertible, $n \geq m$. This puts a lower limit on the radius r_w of the support of the weight function W .

2.3. MLPG formulations

2.3.1. Discontinuity at the interface modelled by a jump function

2.3.1.1. MLPG1. Let ψ defined on Ω_s be a smooth function, and α a constant. For deriving the MLPG1 formulation, we multiply both sides of Equation (1) by $r\psi$, integrate the resulting equations with respect to r over their domains Ω_{s1} and Ω_{s2} of applicability in Ω_s , integrate the second term on the left-hand side of this equation by parts, add $-\alpha\psi(R)(T_2(R, t) - T_0)\sigma_{\bar{\Omega}}$ to it for satisfying the essential boundary condition by the penalty method, and obtain

$$\begin{aligned} & \left[\int_{\Omega_{s1}} \rho_1 c_1 r \frac{\partial T_1}{\partial t} \psi \, dr + \int_{\Omega_{s2}} \rho_2 c_2 r \frac{\partial T_2}{\partial t} \psi \, dr \right] + \left[\int_{\Omega_{s1}} r \kappa_1 \frac{\partial T_1}{\partial r} \frac{\partial \psi}{\partial r} \, dr + \int_{\Omega_{s2}} r \kappa_2 \frac{\partial T_2}{\partial r} \frac{\partial \psi}{\partial r} \, dr \right] \\ & - \alpha \psi(R)(T_2(R) - T_0)\sigma_{\bar{\Omega}} = \left[\int_{\Omega_{s1}} h r \psi \, dr + \int_{\Omega_{s2}} h r \psi \, dr \right] + \left[r \kappa_1 \frac{\partial T_1}{\partial r} \psi \right]_{\Gamma_{s1}} + \left[r \kappa_2 \frac{\partial T_2}{\partial r} \psi \right]_{\Gamma_{s2}} \end{aligned} \tag{12}$$

Here

$$\begin{aligned} \Omega_s &= \Omega_{s1} \cup \Omega_{s2}, \quad \Omega_{s1} \subset [0, b], \quad \Omega_{s2} \subset [b, R] \\ \sigma_{\bar{\Omega}} &= \begin{cases} 1, & r = R \\ 0, & r \neq R \end{cases} \end{aligned} \tag{13}$$

and Γ_{s1} and Γ_{s2} are boundaries of Ω_{s1} and Ω_{s2} , respectively. Furthermore α is a penalty parameter used to enforce the essential boundary condition (2)₄ and has units of κ .

Instead of approximating the temperature field by Equation (4), we follow Krongauz and Belytschko [24] and set

$$T^h(r, t) = \sum_{j=1}^N \phi_j(r) \hat{T}_j(t) + q(t) \chi(r) \tag{14}$$

where q is the amplitude of the jump in $\partial T^h / \partial r$ at $r = b$, and the jump function χ is continuous and differentiable on the entire domain $[0, R]$ except at the point $r = b$ where its first derivative is discontinuous. The jump function χ ensures the continuity of the heat flux at the interface $r = b$ between the two materials without affecting the continuity of the temperature field. The continuity condition (2)₂ gives

$$q(t) = \frac{\kappa_2 - \kappa_1}{\kappa_1 \chi'(b^-) - \kappa_2 \chi'(b^+)} \sum_{i=1}^N \phi'_i(b) \hat{T}_i(t) \tag{15}$$

where a prime denotes differentiation with respect to r . Substitution from (15) into (14) yields

$$T^h(r, t) = \sum_{j=1}^N \tilde{\phi}_j(r) \hat{T}_j(t) \tag{16}$$

where

$$\tilde{\phi}_j(r) = \phi_j(r) + \frac{\kappa_2 - \kappa_1}{\kappa_1 \chi'(b^-) - \kappa_2 \chi'(b^+)} \phi'_j(b) \chi(r) \tag{17}$$

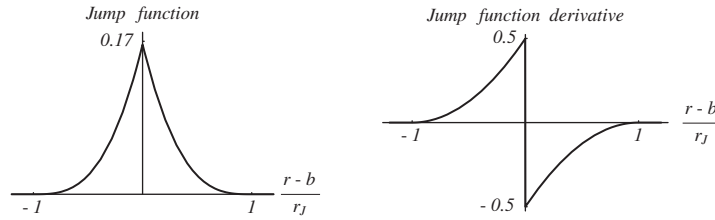


Figure 2. Plot of the jump function, $\chi((r - b)/r_J)$, and its derivative.

We take

$$\chi(r) = \begin{cases} \frac{1}{6} - \frac{1}{2} \left(\frac{|r - b|}{r_J} \right) + \frac{1}{2} \left(\frac{|r - b|}{r_J} \right)^2 - \frac{1}{6} \left(\frac{|r - b|}{r_J} \right)^3, & |r - b| \leq r_J \\ 0, & |r - b| > r_J \end{cases} \quad (18)$$

Thus the size of the support of the jump function χ equals $2r_J$. The jump function (18) and its derivative $\chi'(r)$ with respect to the normalized coordinate $(r - b)/r_J$, are plotted in Figure 2. It is evident that $\chi'(r)$ suddenly goes from 0.5 at $r = b^-$ to -0.5 at $r = b^+$, and $\tilde{\phi}_j(r) = \phi_j(r) - 2\phi'_j(b)\chi(r)$.

When using MLPG1, we set $\psi(r) = \bar{W}_k = W(r - r_k) / \sum_{i=1}^N W(r - r_i)$ with r_w in Equation (7) set equal to r_{ws} , and $\Omega_s = [r_k - 0.5r_{ws}, r_k + 0.5r_{ws}]$. Substitution from (16) into (12) gives

$$\sum_{i=1}^N M_{ki} \hat{T}_i + \sum_{i=1}^N K_{ki} \hat{T}_i = F_k, \quad k = 1, 2, \dots, N \quad (19)$$

where

$$\begin{aligned} M_{ki} &= \int_{\Omega_{s1}} \rho_1 c_1 r \bar{W}_k \tilde{\phi}_i \, dr + \int_{\Omega_{s2}} \rho_2 c_2 r \bar{W}_k \tilde{\phi}_i \, dr \\ K_{ki} &= \int_{\Omega_{s1}} r \kappa_1 \frac{d\bar{W}_k}{dr} \frac{d\tilde{\phi}_i}{dr} \, dr + \int_{\Omega_{s2}} r \kappa_2 \frac{d\bar{W}_k}{dr} \frac{d\tilde{\phi}_i}{dr} \, dr - \alpha \psi_k(R) \sigma_{\bar{\Omega}} \tilde{\phi}_i(R) + R \kappa_2 \frac{d\tilde{\phi}_i}{dr}(R) \bar{W}_k(R) \\ F_k &= -\alpha W_k(R) \sigma_{\bar{\Omega}} T_0 + \int_{\Omega_{s1}} h r W_k \, dr + \int_{\Omega_{s2}} h r \bar{W}_k \, dr \end{aligned} \quad (20)$$

Note that the last two terms on the right-hand side of Equation (12) identically vanish for test functions that vanish at $r = R$. In this formulation it is not necessary to locate a node at the interface $r = b$. \mathbf{M} may be called the heat capacity matrix, \mathbf{K} the thermal conductivity matrix, and \mathbf{F} the thermal load vector. Because of the presence of r in the integrands of the heat capacity and the thermal conductivity matrices, the entries in \mathbf{M} and \mathbf{K} are small for nodes near the centre of the disk and large for nodes near the outer periphery of the disk. Therefore, the condition numbers of the heat capacity and the thermal conductivity matrices are influenced by the outer radius of the disk. Matrices \mathbf{M} and \mathbf{K} are neither symmetric nor banded but are sparse; the sparsity depends upon the node numbering scheme and the support of the weight function W_k used to find the MLS basis functions. The heat capacity matrix \mathbf{M} is not necessarily positive definite.

2.3.1.2. *MLPG5*. For deriving the MLPG5 formulation, we multiply both sides of Equations (1)₁ and (1)₂ by rH_{Ω_s} where H_{Ω_s} is the Heaviside unit step function on Ω_s . Thus H_{Ω_s} equals zero at points exterior to Ω_s . We integrate the resulting equations with respect to r on Ω_{s1} and Ω_{s2} , add their respective sides, add $-\alpha(T_2(R, t) - T_0)\sigma_{\bar{\Omega}}$ to it and arrive at

$$\begin{aligned} & \left[\int_{\Omega_{s1}} \rho_1 c_1 r \frac{\partial T}{\partial t} dr + \int_{\Omega_{s2}} \rho_2 c_2 r \frac{\partial T}{\partial t} dr \right] - \left[r\kappa_1 \frac{\partial T}{\partial r} \right]_{\Gamma_{s1}} - \left[r\kappa_2 \frac{\partial T}{\partial r} \right]_{\Gamma_{s2}} \\ & - \alpha(T_2(R) - T_0)\sigma_{\bar{\Omega}} = \int_{\Omega_{s1}} hr dr + \int_{\Omega_{s2}} hr dr \end{aligned} \quad (21)$$

Substitution from (16) into (21) yields (19) with

$$M_{ki} = \int_{\Omega_{s1}} \rho_1 c_1 r \tilde{\phi}_i dr + \int_{\Omega_{s2}} \rho_2 c_2 r \tilde{\phi}_i dr \quad (22)$$

$$K_{ki} = - \left[r\kappa_1 \frac{d\tilde{\phi}_i}{dr} \right]_{\Gamma_{s1}} - \left[r\kappa_2 \frac{d\tilde{\phi}_i}{dr} \right]_{\Gamma_{s2}} - \alpha\sigma_{\bar{\Omega}} \tilde{\phi}_i(R) \quad (23)$$

$$F_k = -\alpha\sigma_{\bar{\Omega}}T_0 + \int_{\Omega_{s1}} hr dr + \int_{\Omega_{s2}} hr dr \quad (24)$$

Note that Ω_s varies with k .

The heat capacity matrix \mathbf{M} and the thermal conductivity matrix \mathbf{K} given by (22) and (23), respectively, are neither symmetric nor positive definite.

2.3.2. *Continuity of heat flux at the interface accounted by a Lagrange multiplier*. In this case it is necessary to place two overlapping nodes at the interface $r = b$, one for each material, and the weak form (12) is replaced by

$$\begin{aligned} & \left[\int_{\Omega_{s1}} \rho_1 c_1 r \frac{\partial T_1}{\partial t} \psi_1 dr + \int_{\Omega_{s2}} \rho_2 c_2 r \frac{\partial T_2}{\partial t} \psi_2 dr \right] + \left[\int_{\Omega_{s1}} r\kappa_1 \frac{\partial T_1}{\partial r} \frac{d\psi_1}{dr} dr + \int_{\Omega_{s2}} r\kappa_2 \frac{\partial T_2}{\partial r} \frac{d\psi_2}{dr} dr \right] \\ & - \delta\lambda(T_2(R) - T_0) - \lambda\psi_2(R) - \delta\gamma(T_2(b^+) - T_1(b^-)) - \gamma(\psi_2(b) - \psi_1(b)) \\ & = \left[\int_{\Omega_{s1}} hr\psi_1 dr + \int_{\Omega_{s2}} hr\psi_2 dr \right] \end{aligned} \quad (25)$$

Here λ and γ are Lagrange multipliers that enforce essential boundary conditions at $r = R$, and the continuity of the temperature at the interface $r = b$, respectively, and ψ_1 and ψ_2 are test functions defined on Ω_{s1} and Ω_{s2} . Note that the Lagrange multiplier γ enforces the continuity of temperature at $r = b$, and the continuity of the heat flux is weakly satisfied. Equation (25) must hold for all $\delta\lambda$, $\delta\gamma$, ψ_1 and ψ_2 . Euler's equations associated with (25) are Equations (1) and boundary and continuity conditions (2), and $\lambda = \kappa_2 R(\partial T_2/\partial r)(R, t)$. For computational purposes, heat conduction problems in $[0, b]$ and $[b, R]$ are essentially formulated separately and the Lagrange multipliers connect the two. The temperature field on Ω_s is approximated

by (10). There are $N + 2$ unknowns: the fictitious temperature \hat{T} at N nodes and the two Lagrange multipliers λ and γ . Equations for their determination are

$$\begin{aligned} \sum_{i=1}^N (M_{ki} \dot{\hat{T}}_i + K_{ki} \hat{T}_i) + G_k \gamma + L_k \lambda &= F_k, \quad k = 1, 2, \dots, N \\ \sum_{i=1}^N \Gamma_i \hat{T}_i &= 0, \quad \sum_{i=1}^n \Lambda_i \hat{T}_i = T_0 \end{aligned} \quad (26)$$

where the heat capacity matrix \mathbf{M} and the conductivity matrix \mathbf{K} are given by Equations (20)₁ and (20)₂, respectively, with $\tilde{\phi}_i$ replaced by ϕ_i and the load vector \mathbf{F} by Equation (20)₃ with the α term omitted. Using the additional subscript 1 on Γ_{1i} and Λ_{1i} etc. to denote their values for the domain Ω_{s1} , we set

$$\begin{aligned} G_{1k} &= \bar{W}_1(b - r_k), \quad G_{2k} = -\bar{W}_2(b - r_k) \\ L_{1k} &= 0, \quad L_{2k} = -\bar{W}_2(R - r_k) \\ \Gamma_{1i} &= \phi_{1i}(b), \quad \Gamma_{2i} = -\phi_{2i}(b), \quad \Lambda_{1i} = 0, \quad \Lambda_{2i} = \phi_{2i}(R) \end{aligned} \quad (27)$$

While evaluating the mass and the stiffness matrices for nodes in $\Omega_{s1}(\Omega_{s2})$, contributions from nodes in $\Omega_{s2}(\Omega_{s1})$ do not appear.

When using MLPG5, we take ψ_1 and ψ_2 equal to the Heaviside unit step functions defined on Ω_{s1} and Ω_{s2} . Contributions to the conductivity matrix from the derivatives at $r = b$ and at $r = R$ of the Heaviside function are zeros.

Note that there are no $\dot{\lambda}$ and $\dot{\gamma}$ terms in Equations (26). However, Equations (26) can be written in the form of Equations (19) by including zeros in rows and columns corresponding to variables $\dot{\lambda}$ and $\dot{\gamma}$. This makes the mass matrix singular. One way to eliminate these two rows of zero elements in \mathbf{M} is to solve Equations (26)₂ and (26)₃ for \hat{T}_N and \hat{T}_M where M is the node at $r = b$ belonging to the material of the inner disk. Substituting for \hat{T}_N and \hat{T}_M in Equations (26)₁ and renumbering the N unknowns will make \mathbf{M} non-singular.

2.4. The time integration scheme

We use the generalized trapezoidal algorithm [26] to integrate the coupled first-order ordinary differential Equations (19). Recursive relations relating $\hat{\mathbf{T}}$ and $\dot{\hat{\mathbf{T}}}$ at times t_n and t_{n+1} are

$$\begin{aligned} \mathbf{M} \dot{\hat{\mathbf{T}}}_{n+1} + \mathbf{K} \hat{\mathbf{T}}_{n+1} &= \mathbf{F}_{n+1} \\ \hat{\mathbf{T}}_{n+1} &= \hat{\mathbf{T}}_n + \Delta t \hat{\mathbf{T}}_{n+\beta} \\ \dot{\hat{\mathbf{T}}}_{n+\beta} &= (1 - \beta) \dot{\hat{\mathbf{T}}}_n + \beta \dot{\hat{\mathbf{T}}}_{n+1} \end{aligned} \quad (28)$$

where $\hat{\mathbf{T}}_n$ and $\dot{\hat{\mathbf{T}}}_n$ are approximations of $\hat{\mathbf{T}}(t_n)$ and $\dot{\hat{\mathbf{T}}}(t_n)$, respectively, $\mathbf{F}_{n+1} = \mathbf{F}(t_{n+1})$, Δt is the time step, and $\beta \in [0, 1]$ is a parameter. For symmetric and positive definite matrices \mathbf{M} and \mathbf{K} , the integration scheme (28) is unconditionally stable for $\beta \geq \frac{1}{2}$. For $\beta < \frac{1}{2}$,

the algorithm is conditionally stable and one must take

$$\Delta t < \frac{2}{(1 - 2\beta)\hat{\lambda}_{\max}} \quad (29)$$

where $\hat{\lambda}_{\max}$ is the maximum eigenvalue of

$$(\mathbf{M} - \hat{\lambda}\mathbf{K})\hat{\mathbf{T}} = \mathbf{0} \quad (30)$$

For $\beta = 0$ and \mathbf{M} a diagonal matrix, algorithm (28) is explicit; otherwise it is implicit. The heat capacity matrix \mathbf{M} can be diagonalized by using the row-sum technique in which the diagonal element M_{ii} equals the sum of entries in the i th row of \mathbf{M} .

3. COMPUTATION AND DISCUSSION OF RESULTS

A computer code based on the four aforesaid formulations has been developed. Results have been computed for the following values of material and geometric parameters.

$$\begin{aligned} \rho_1 = \rho_2 = 10 \text{ g/cm}^3, \quad c_1 = c_2 = 0.1 \text{ cal K}^{-1} \text{ g}^{-1}, \quad \kappa_1 = 2 \text{ cal s}^{-1} \text{ cm}^{-1} \text{ K}^{-1} \\ T_0 = 273 \text{ K}, \quad \kappa_2 = 0.5 \text{ cal s}^{-1} \text{ cm}^{-1} \text{ K}^{-1}, \quad h = 2 \text{ cal cm}^{-3} \text{ s}^{-1} \\ R = 10 \text{ cm}, \quad b = 4 \text{ cm}, \quad \alpha = 10^6 \text{ cal/(s K cm)} \end{aligned} \quad (31)$$

Complete monomials of degree 1 (i.e. $m = 2$ in Equation (4)) are used to generate the MLS basis functions ϕ_i . Figures 3(a) and (b) depict the placement of 20 nodes when the discontinuity in the temperature gradient is modelled by the jump function and the method of Lagrange multipliers. In the latter case two overlapping nodes are located at $r = b$; one of these nodes belongs to material 1 and the other to material 2. Equal number of nodes are uniformly placed in $[0, b]$ and in $[b, R]$. For the method employing the jump function, nodes are equally spaced on $[0, R]$ with $r_k = R(k - 1)/(N - 1)$ giving the radial co-ordinate of node k , $k = 1, 2, \dots, N$. The radius r_w of the support of the weight function $W_k(r) = W(r - r_k)$ is taken to equal $1.63R/(N - 1)$ for $k = 2, 3, \dots, N - 1$; and $3.26R/(N - 1)$ for $k = 1$ and N .

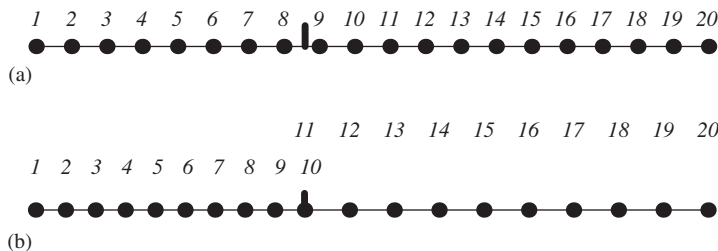


Figure 3. Location of nodes for the method of: (a) the jump function; and (b) the Lagrange multipliers.

When using MLPG5, we set

$$\begin{aligned}\Omega_1 &= [r_1, r_3] \\ \Omega_k &= \left[r_k - \frac{R}{2(N-1)}, r_k + \frac{R}{2(N-1)} \right], \quad k = 2, 3, \dots, N-1 \\ \Omega_N &= [r_{N-2}, r_N]\end{aligned}\quad (32)$$

For the method of Lagrange multipliers, the subdomains and the supports of the weight and the test functions are selected in the same way as for the method of the discontinuity function.

Unless otherwise specified, 12 quadrature points are used to numerically evaluate integrals over each subdomain, and 20 nodes are used to compute all of the results. A convergence study for the number of nodes and the number of quadrature points is performed.

3.1. Steady-state heat conduction

For steady-state heat conduction, the analytical solution of the problem is

$$T(r) = \begin{cases} T_0 + \frac{hR^2}{4\kappa_2} - \frac{hr^2}{4\kappa_1} + \frac{b^2h}{4} \left(\frac{1}{\kappa_1} - \frac{1}{\kappa_2} \right), & 0 \leq r \leq b \\ T_0 + \frac{h}{4\kappa_2} (R^2 - r^2), & b \leq r \leq R \end{cases} \quad (33)$$

In order to demonstrate the need for using either a jump function or the method of Lagrange multipliers for modelling the discontinuity in the temperature gradient at the interface $r = 4$ cm, we have plotted in Figure 4(a)–(c) the variation with r of the temperature gradient computed with and without the use of these methods. It is transparent from these plots that one of the two methods needs to be employed for accurately modelling the discontinuity in the temperature gradient at $r = 4$ cm. However, the temperature gradient computed at points away from $r = 4$ cm without employing either one of the two methods is close to that obtained from the analytical solution of the problem. The computed solution for different cases is compared with the analytical solution in Figures 5–7. In each case, results computed with the discontinuity in the temperature gradient modelled by a jump function and those obtained by the method of Lagrange multipliers are presented in parts (a) and (b) of a figure.

The computed radial distribution of the temperature is compared with that obtained from the analytical solution in Figure 5. It is clear that the MLPG1 and the MLPG5 formulations and the two techniques of modelling discontinuity in the temperature gradient give results very close to the analytical solution. It follows from the results plotted in Figures 6 and 7 that for the MLPG1 formulation and the jump function used to model the discontinuity in the temperature gradient, the H^0 and the H^1 norms of the error defined as

$$(H^0(e))^2 = \frac{\int_0^R (T_{\text{anal}} - T_{\text{num}})^2 dr}{\int_0^R T_{\text{anal}}^2 dr} \quad (34)$$

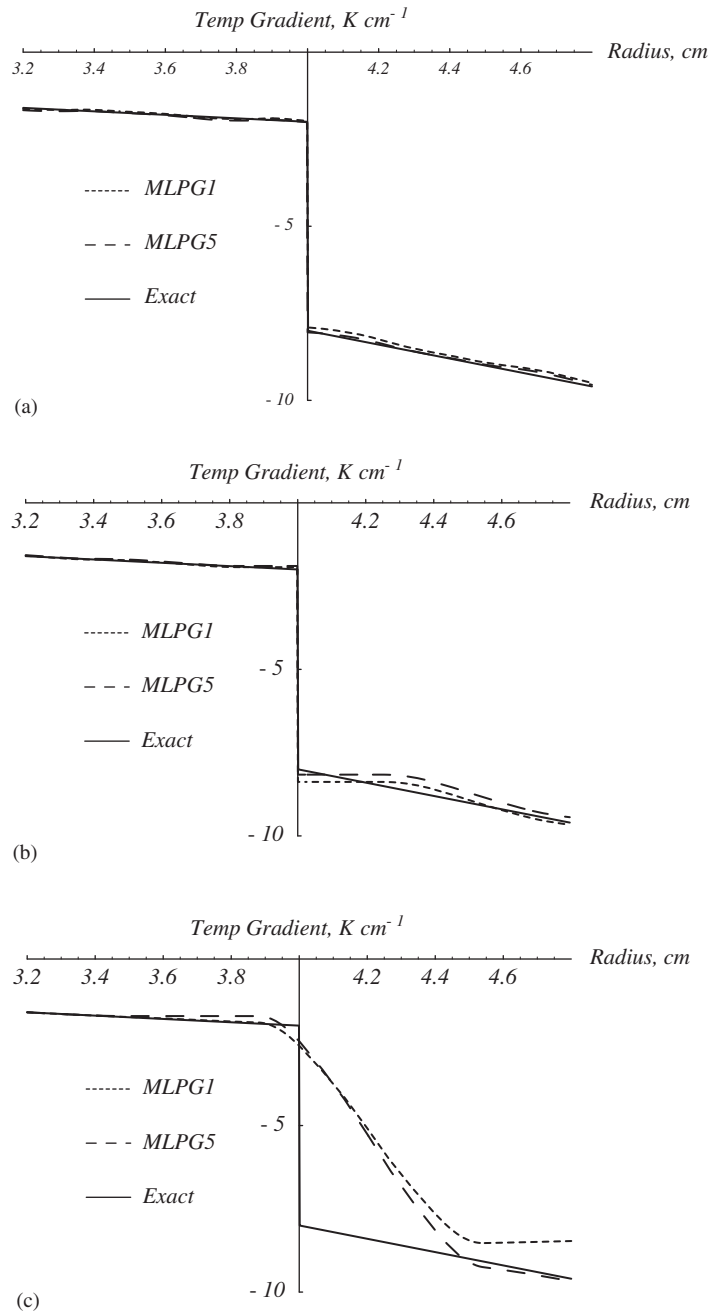


Figure 4. Radial distribution of the temperature gradient at points near the interface $r = 4$ cm between the two materials computed: (a) with the use of the jump function; (b) with the method of Lagrange multipliers; and (c) without the use of these methods.

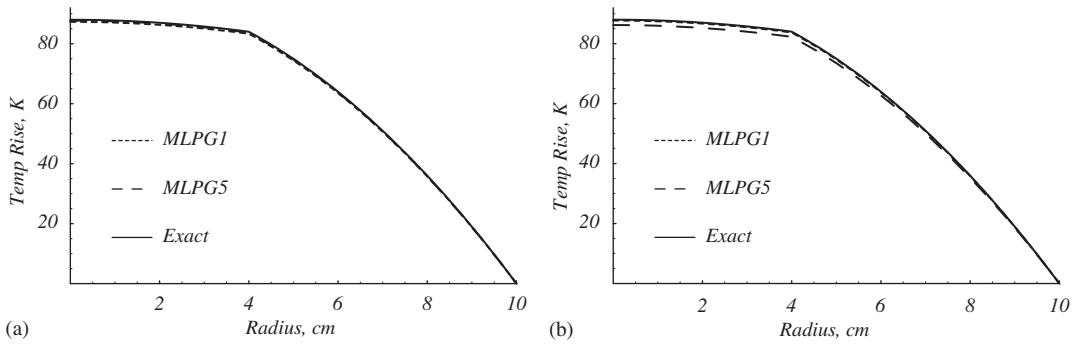


Figure 5. Steady-state radial distribution of the temperature rise computed with the method of: (a) jump function; and (b) Lagrange multipliers.

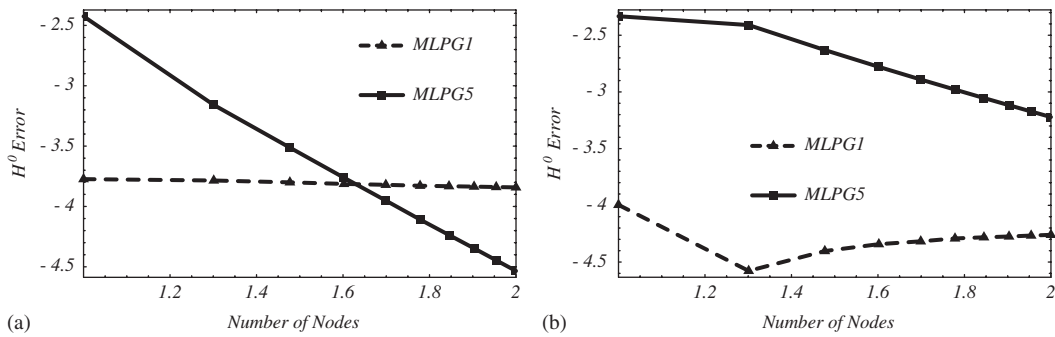


Figure 6. Variation with the number of nodes of the H^0 norm of the error in the temperature computed with the method of: (a) jump function; and (b) Lagrange multipliers. Note that the plot is on a \log_{10} - \log_{10} scale.

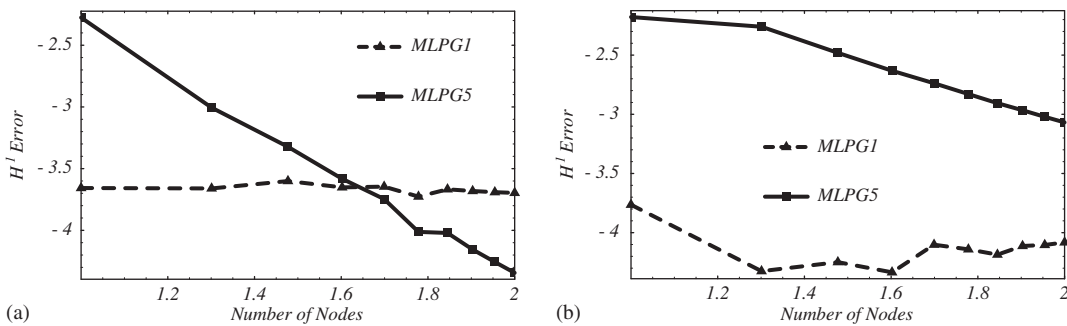


Figure 7. Variation with the number of nodes of the H^1 norm of the error in the temperature computed with the method of: (a) jump function; and (b) Lagrange multipliers. Note that the plot is on a \log_{10} - \log_{10} scale.

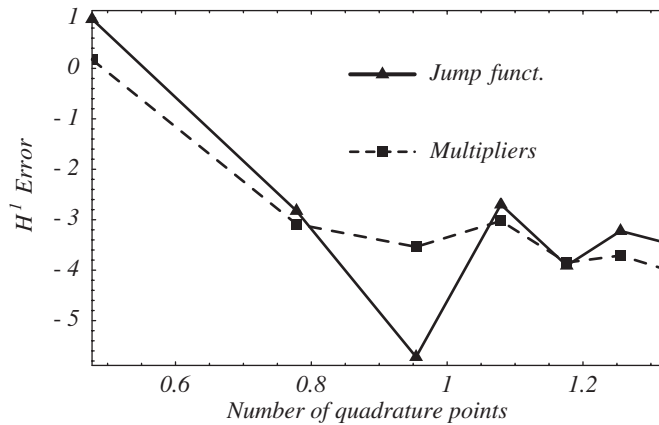


Figure 8. For the MLPG1, variation with the number of quadrature points of the H^1 norm of the error in the temperature computed with methods of the jump function and the Lagrange multipliers. Note that the plot is on a \log_{10} - \log_{10} scale.

$$(H^1(e))^2 = \frac{\int_0^R [(T_{\text{anal}} - T_{\text{num}})^2 + R^2(T'_{\text{anal}} - T'_{\text{num}})^2] dr}{\int_0^R [T_{\text{anal}}^2 + R^2(T'_{\text{anal}})^2] dr} \quad (35)$$

where $T' = \partial T / \partial r$, remain unchanged with an increase in the number of nodes, but this is not the case for the method of Lagrange multipliers. For the same number of nodes, the error is lower for the method of Lagrange multipliers than that with the method employing the jump function. With the MLPG5 formulation and for total number of nodes exceeding 20, the error decreases monotonically with an increase in the number of nodes irrespective of the method used to model the jump in the temperature gradient at $r = 4$ cm. The rate of convergence equals 2 for the H^0 error, and 2 for the H^1 error with the discontinuity in the temperature gradient modelled by a jump function and is only 0.5 for the method of Lagrange multipliers. In general, for the same number of nodes, the MLPG1 formulation gives a lower value of H^0 and H^1 error than the MLPG5 formulation; the trend is reversed for the number of nodes exceeding 40 and the jump function employed to model a discontinuity in the temperature gradient.

For the steady heat conduction in a homogeneous disk and the MLPG5 formulation only seven nodes and three integration points over each subdomain gave results essentially overlapping the analytical solution of the problem.

Results plotted in Figure 8 evince that a minimum of twelve integration points ought to be employed to numerically evaluate integrals appearing in the weak formulation of the problem; this holds for both the MLPG1 and the MLPG5 formulations and also for either one of the two methods to simulate the discontinuity in the temperature gradient at $r = 4$ cm.

3.1.1. Summary of results. Table I summarizes our findings for the two MLPG formulations and the two methods of accounting for the discontinuity in the temperature gradient.

Table I. Comparison of results from MLPG1 and MLPG5 methods.

	MLPG1		MLPG5	
	Jump function	Lagrange multipliers	Jump function	Lagrange multipliers
Convergence rate of error in H^1 -norm with an increase in the number, n_{nodes} , of nodes	0	0 for $n_{\text{nodes}} > 20$	2	1.0 for $n_{\text{nodes}} > 20$
Convergence rate of error in H^1 -norm with an increase in the number, n_{int} , of integration points	Variable for $n_{\text{int}} < 12$ 0 for $n_{\text{int}} > 12$	10 for $n_{\text{int}} < 6$ 0 for $n_{\text{int}} > 6$	—	—
Recommended minimum number of integration points	16	7	16	7

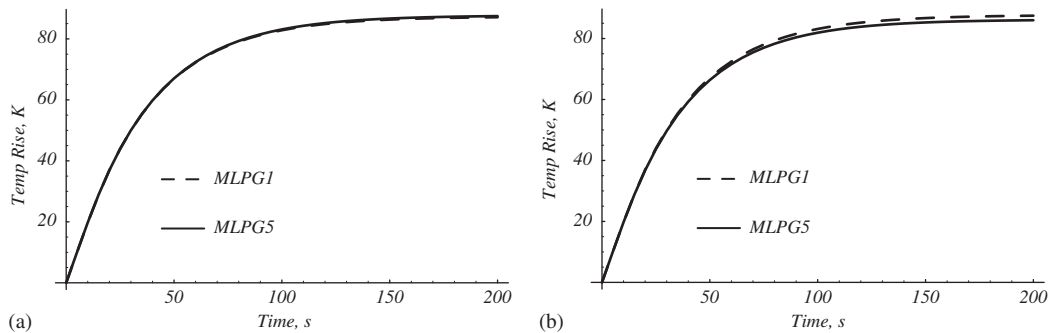


Figure 9. Time history of the temperature rise at the disk centroid computed with the method of: (a) the jump function; and (b) the Lagrange multipliers.

3.2. Transient heat conduction

In order to compute results for the transient problem, we set $\beta = \frac{2}{3}$ in Equation (28) and use the consistent heat capacity matrix. Thus the integration method is implicit and unconditionally stable. Figures 9–11 exhibit, respectively, the time histories of the temperature at the centre of the disk, the jump in the temperature gradient at the interface $r = 4$ cm, and the heat flux ($\kappa R \partial T / \partial r$) at the outer edge $r = 10$ cm of the disk. The MLPG1 and the MLPG5 formulations give virtually identical results with the method of the jump function, and very close results with the method of Lagrange multipliers.

3.3. Comparison of MLPG, EFG and FE methods

Table II provides a comparison of the MLPG, the element free Galerkin (EFG) and the finite element (FE) methods.

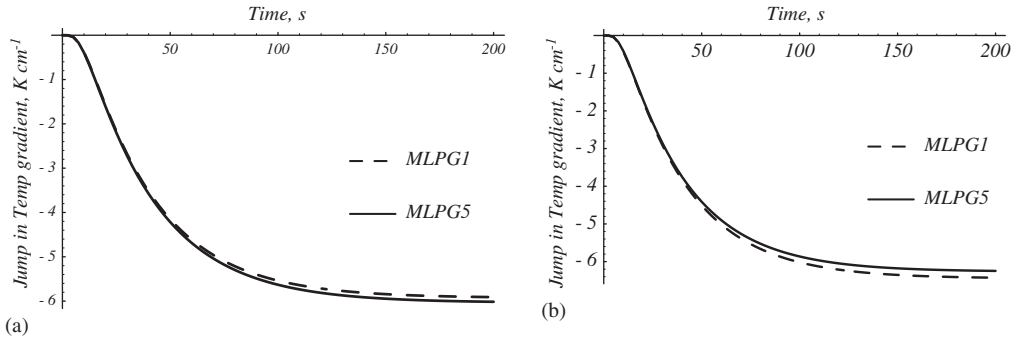


Figure 10. Time history of the jump in the temperature gradient at the interface $r = 4$ cm computed with the method of: (a) the jump function; and (b) the Lagrange multipliers.

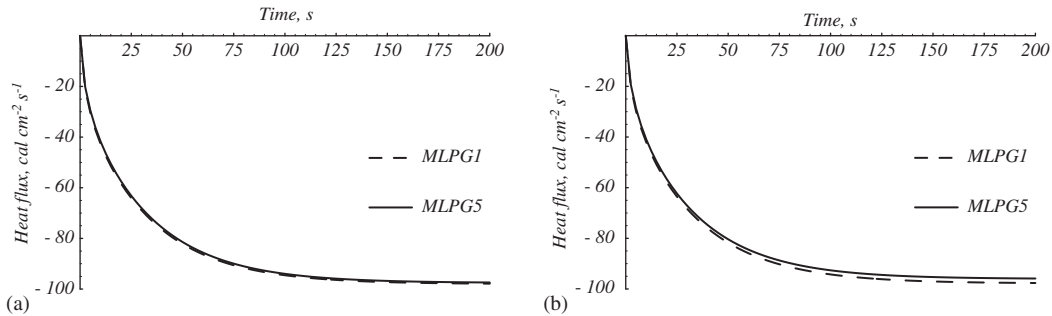


Figure 11. Time history of the heat flux at the outer edge ($r = 10$ cm) computed with the method of: (a) the jump function; and (b) the Lagrange multipliers.

4. CONCLUSIONS

We have analysed axisymmetric heat conduction in a bimetallic circular disk with two, MLPG1 and MLPG5, meshless local Petrov–Galerkin formulations. For each MLPG method, the discontinuity in the temperature gradient at the interface is satisfied either by using a jump function or by the method of Lagrange multipliers. For the steady-state heat conduction, the four computed radial distributions of the temperature agree very well with the analytic solution of the problem. Also, the jump in the temperature gradient at the interface $r = b$ between the two materials computed from each numerical solution matches well with that from the analytical solution. With an increase in the number of equally spaced nodes, the H^0 and the H^1 norms of the error in the computed temperature field decrease monotonically for the MLPG5 method but are essentially unaffected for the MLPG1 method. For the same error in H^1 norm, less number of integration points are needed for the method of Lagrange multipliers than with the method employing the jump function. The two MLPG formulations yield virtually identical results for the transient heat conduction problem.

Table II. Comparison of the MLPG, the FE, and the EFG methods for a transient linear problem.

	MLPG	FEM	EFG
Weak form	Local	Global	Global
Information needed about nodes	Locations only	Locations and connectivity	Locations and connectivity
Subdomains	Circular/rectangular, not necessarily disjoint	Polygonal and disjoint	Polygonal and disjoint
Basis functions	Complex and difficult to express in closed form	Simple polynomials	Complex and difficult to express in closed form
Integration rule	Higher order	Lower order	Higher order
Satisfaction of essential boundary conditions	Requires extra effort	Easy to enforce	Requires additional effort
Mass/stiffness matrices	Asymmetric, large band width that cannot be determined <i>a priori</i> , not necessarily positive semidefinite	Symmetric, banded, mass matrix positive definite, stiffness matrix positive definite after imposition of essential boundary conditions.	Symmetric, large band width that cannot be determined <i>a priori</i>
Sum of elements of mass matrix	Not necessarily equal to the total mass of the body	Equals total mass of the body	Not necessarily equal to the total mass of the body
Assembly of equations	Not required	Required	Not required
Stress/strains	Smooth everywhere	Good at integration points	Smooth everywhere
Locking phenomenon for constrained problems	No	Yes	No
Addition of nodes	Easy	Difficult	Difficult
Determination of time step size for stability in an explicit algorithm	Difficult, requires determination of the maximum frequency of the structure	Relatively easy	Difficult, requires determination of the maximum frequency of the structure
Computation of the total strain energy of the body	Difficult	Easy	Easy
Analysis of a biomaterial body	Requires either consideration in the generation of basis functions or the use of Lagrange multipliers or the jump function	Easy to implement	Requires either consideration in the generation of basis functions or the use of Lagrange multipliers or the jump function
Data preparation effort	Little	Extensive	Extensive

For each MLPG formulation, the two methods of accounting for the continuity of the temperature and the normal component of the heat flux at the interface between two adjoining distinct materials can be extended to two- and three-dimensional thermomechanical problems.

REFERENCES

1. Belytschko T, Lu YY, Gu L. Element-free Galerkin methods. *International Journal for Numerical Methods in Engineering* 1994; **37**:229–256.
2. Duarte CA, Oden JT. H - p clouds—an hp meshless method. *Numerical Methods for Partial Differential Equations* 1996; **12**:673–705.
3. Liu W, Jun S, Zhang Y. Reproducing kernel particle method. *International Journal for Numerical Methods in Fluids* **20**:1081–1106.
4. Lucy LB. A numerical approach to the testing of the fission hypothesis. *The Astronomical Journal* 1977; **82**(12):1013–1024.
5. Nayroles B, Touzot G, Villon P. Generalizing the finite element method: diffuse approximation and diffuse elements. *Computational Mechanics* 1992; **10**:307–318.
6. Melenk JM, Babuska I. The partition of unity finite element method: Basic theory and applications. *Computer Methods in Applied Mechanics and Engineering* 1996; **139**:289–314.
7. Sukumar N, Moran B, Belytschko T. The natural element method in solid mechanics. *International Journal for Numerical Methods in Engineering* 1998; **43**:839–887.
8. Wendland H. Piecewise polynomial, positive definite and compactly supported radial basis functions of minimal degree. *Advances in Computational Methods* 1995; **4**:389–396.
9. Atluri SN, Zhu T. A new meshless local Petrov–Galerkin (MLPG) approach in computational mechanics. *Computational Mechanics* 1998; **22**(2):117–127.
10. Zhang GM, Batra RC. Modified smoothed particle hydrodynamics method and its application to transient problems. *Computational Mechanics* 2004; **34**:137–146.
11. Lancaster P, Salkauskas K. Surfaces generated by moving least squares methods. *Mathematics of Computation* 1981; **37**:141–158.
12. Atluri SN, Shen SP. The meshless local Petrov–Galerkin (MLPG) method: a simple and less-costly alternative to the finite element methods. *Computer Modeling in Engineering and Sciences* 2002; **3**(1):11–51.
13. Qian LF, Batra RC, Chen LM. Elastostatic deformations of a thick plate by using a higher-order shear and normal deformable plate theory and two meshless local Petrov–Galerkin (MLPG) methods. *Computer Modeling in Engineering and Sciences* 2003; **4**:161–176.
14. Batra RC, Vidoli S. Higher order piezoelectric plate theory derived from a three-dimensional variational principle. *AIAA Journal* 2002; **40**(1):91–104.
15. Raju IS, Phillips DR. Further developments in the MLPG method for beam problems. *Computer Modeling in Engineering and Sciences* 2003; **4**:141–159.
16. Xiao JR, McCarthy MA. A local Heaviside weighted meshless method for two-dimensional solids using radial basis functions. *Computational Mechanics* 2003; **31**:301–315.
17. Gu YT, Liu GR. A meshless local Petrov–Galerkin (MLPG) method for free and forced vibration analysis for solids. *Computational Mechanics* 2000; **27**:188–198.
18. Batra RC, Ching H-K. Analysis of elastodynamic deformations near a crack-notch tip by the meshless local Petrov–Galerkin (MLPG) Method. *Computer Modeling in Engineering and Sciences* 2002; **3**:717–730.
19. Qian LF, Batra RC, Chen LM. Free and forced vibrations of thick rectangular plates by using higher-order shear and normal deformable plate theory and meshless local Petrov–Galerkin (MLPG) method. *Computer Modeling in Engineering and Sciences* 2003; **4**:519–534.
20. Qian LF, Batra RC. Design of bidirectional functionally graded plate for optimal natural frequency. *Journal of Sound and Vibration* 2004; in press.
21. Qian LF, Batra C, Chen LM. Static and dynamic deformations of thick functionally graded elastic plate by using higher-order shear and normal deformable plate theory and meshless local Petrov–Galerkin method. *Composites: Part B* 2004; **35**:685–697.
22. Qian LF, Batra RC. Transient thermoelastic deformations of a thick functionally graded plate. *Journal of Thermal Stresses* 2004; **27**:705–740.
23. Cordes LW, Moran B. Treatment of material discontinuity in the Element-Free Galerkin method. *Computer Methods in Applied Mechanics and Engineering* 1996; **139**:75–89.

24. Krongauz Y, Belytschko T. EFG approximation with discontinuous derivatives. *International Journal for Numerical Methods in Engineering* 1998; **41**:1215–1233.
25. Warlock A, Ching HK, Kapila AK, Batra RC. Plane strain deformations of an elastic material compressed in a rough rectangular cavity. *International Journal of Engineering Science* 2002; **40**:991–1010.
26. Hughes TJR. *The Finite Element Method: Linear Static and Dynamic Finite Element Analysis*. Prentice-Hall: New Jersey, 1987.